

Innovative Bacterial Cellulose and UiO-66 Composites for Superior Zinc Ion Battery Separator Performance

Tian Zhao*, Pengcheng Xiao, Saiqun Nie, Jiangyong Yu, Shilin Peng,
Jiayao Chen, Fuli Luo, Yi Chen*

(School of Packaging and Material Engineering, Hunan University of Technology, Zhuzhou, Hunan 412007)

Experimental part

Materials

The BC aqueous dispersion used in this study has a solids content of 2 wt.% (as specified by the supplier). This concentration ensures uniform nanofiber dispersion while facilitating subsequent DMF solvent exchange and vacuum filtration for film casting-higher concentrations lead to fiber aggregation and non-uniform films, whereas lower concentrations make film thickness difficult to control.

For UiO-66 synthesis, we employed a molar ratio of Zirconium propoxide solution: BDC: acetic acid = 0.6 mmol: 0.9 mmol: 4.5 mmol in a total of 192 mL DMF. This 1: 1.5 metal-to-ligand ratio, together with the elevated acetic acid modulator concentration, enables the formation of uniform UiO-66 nuclei (~50 nm in diameter) at room temperature while preventing over-coordination that would yield overly large or rapidly aggregating crystals. The optimized DMF volume ensures good fluidity of the reaction mixture and thorough wetting of the BC fiber surfaces, ultimately producing highly dispersed UiO-66 particles stably anchored on the BC substrate.

Ionic Conductivity:

GF separators, BC separators, and BC@UiO-66 separators were each assembled into stainless steel symmetrical cells using 2M ZnSO₄ solution as the electrolyte, with two stainless steel electrodes. Electrochemical impedance spectroscopy (EIS) was conducted using a CHI760e electrochemical workstation within a frequency range of 10⁵ to 10⁻² Hz and an amplitude of 10 mV. The impedance values for the cells assembled with GF separators, BC separators, and BC@UiO-66 separators were obtained. The relevant values were then substituted into equation (1-1) to determine the ionic conductivity of the separators (mS cm⁻¹).

$$\sigma = \frac{L}{AR} \quad (1-1)$$

In the formula:

L—thickness of the separator sample (cm);

A—area of the stainless-steel electrode (cm²);

R—impedance value of the separator (mΩ).

Ion Migration Number:

The zinc ion migration number $t_{Zn^{2+}}$ for the separator samples is measured using a CHI760e electrochemical workstation through electrochemical impedance spectroscopy (EIS) and constant potential direct current polarization tests. First, EIS is conducted on a Zn||Zn battery within a frequency range of 10⁵ to 10⁻² Hz with an amplitude of 10 mV. Following this, a constant potential DC polarization test is performed with a polarization voltage of 10 mV and a polarization time of 4000 seconds. Finally, EIS is performed again on the polarized battery under the same conditions.

By analyzing the results from these three tests, parameters necessary for calculating the zinc ion migration number are obtained. These parameters are then substituted into the following formula (1-2) to calculate the zinc ion migration number ($t_{Zn^{2+}}$):

$$t_{Zn^{2+}} = \frac{I_{SS}R_{\Omega,SS}(\Delta V - I_0R_{ct,0})}{I_0R_{\Omega,0}(\Delta V - I_{SS}R_{ct,SS})} \quad (1-2)$$

In the formula:

ΔV—The DC polarization voltage (mV);

I_0 , I_{SS} —The initial and steady-state current values during the constant potential DC polarization test (μA);

$R_{\Omega,0}$, $R_{\Omega,SS}$ —The lower equivalent series resistance values obtained from the Nyquist plot before and after the constant potential DC polarization test (Ω);

$R_{ct,0}$, $R_{ct,SS}$ —The charge transfer resistance values before and after the constant potential DC polarization test (Ω).

Calculation details

All density functional theory (DFT) calculations were carried out in the CP2K code. All calculations employed a mixed Gaussian and planewave basis sets. Core electrons were represented with norm-conserving Goedecker-Teter-Hutter pseudopotentials, and the valence electron wavefunction was expanded in a double-zeta basis set with polarization functions along with an auxiliary plane wave basis set with an energy cutoff of 450 Ry. The generalized gradient approximation exchange-correlation functional of Perdew, Burke, and Enzerhof (PBE) was used. Each configuration was optimized with the Broyden-Fletcher-Goldfarb-Shanno (BGFS) algorithm with SCF convergence criteria of 1.0×10^{-5} au. The van der Waals correction of Grimme's DFT-D3 model was also adopted.

The adsorption energy between the adsorbate and the substrate can be calculated using the following equation:

$$\Delta E_{ads} = E_{adsorbate@substrate} - E_{substrate} - E_{adsorbate} \quad (1)$$

In Eq. 1, $E_{adsorbate@substrate}$ and $E_{substrate}$ represent the total energies of the substrate with and without the adsorption of adsorbate, respectively. $E_{adsorbate}$ is the total energy of the adsorbate. **According to this equation, a negative adsorption energy corresponds to a stable adsorption structure.**

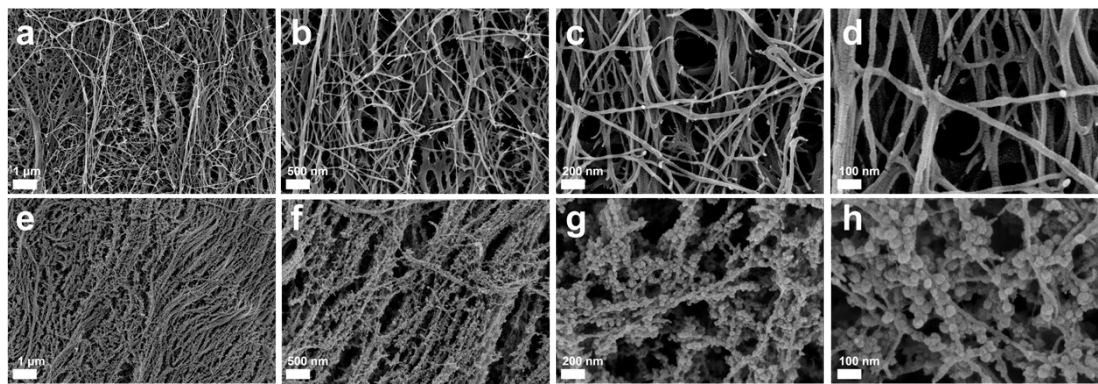


Figure S1. Surface SEM images of the separators: (a) BC separator at 1 μm , (b) BC separator at 500 nm, (c) BC separator at 200 nm, (d) BC separator at 100 nm; (e) BC@UiO-66 separator at 1 μm , (f) BC@UiO-66 separator at 500 nm, (g) BC@UiO-66 separator at 200 nm, (h) BC@UiO-66 separator at 100 nm.

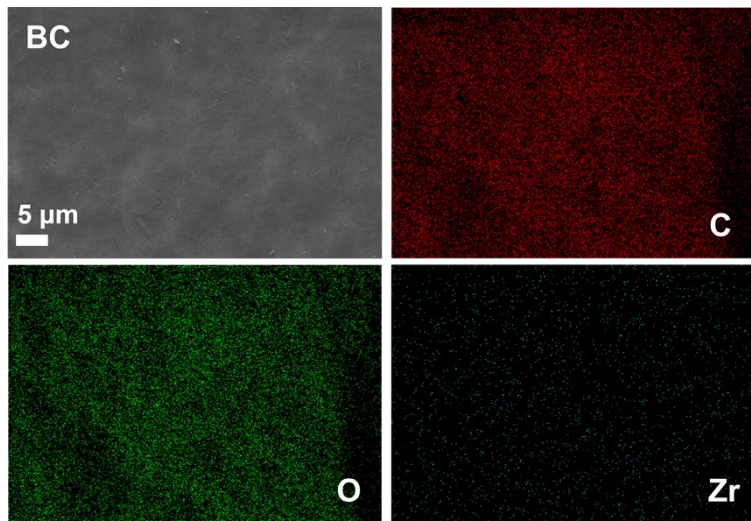


Figure S2. SEM image of BC separator and elemental mapping images for C, O and Zr.

Table S1. Total distribution spectrum map of the BC separator.

Element	Line Type	wt %	wt % Sigma	at %
C	K-line	58.07	0.24	64.85
O	K-line	41.93	0.24	35.15
Zr	L-line	0.00	0.00	0.00
Total		100.00		100.00

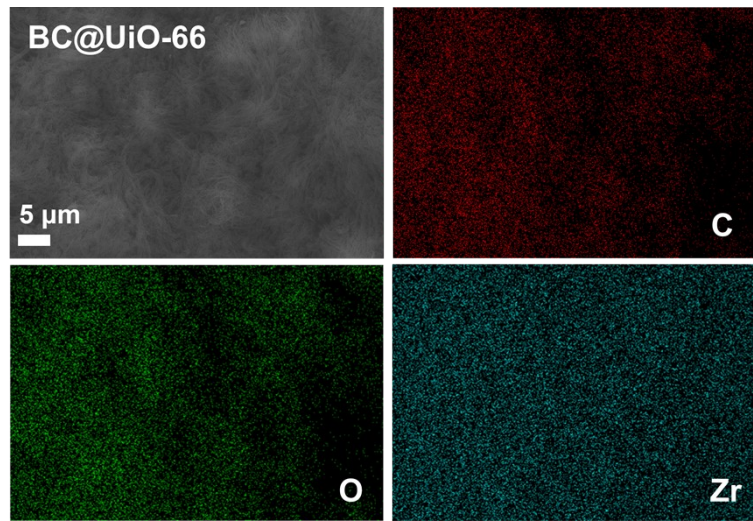


Figure S3. SEM image of BC@UiO-66 separator and elemental mapping images for C, O and Zr.

Table S2. Total distribution spectrum map of the BC@UiO-66 separator.

Element	Line Type	wt %	wt % Sigma	at %
C	K-line	50.50	0.30	66.48
O	K-line	30.61	0.25	30.25
Zr	L-line	18.88	0.21	3.27
Total		100.00		100.00

Table S3. ICP-OES test results for the BC separator.

Sample ID	Analyzed Element	Initial Solution Concentration C ₀ (mg/L)	Digested Solution Concentration C ₁ (mg/L)	Element Content C _x (mg/kg)	Element Content W (%)
BC	Ca	3.4175	3.4175	791.0852	0.0791%
BC	K	0.6855	0.6855	158.6816	0.0159%
BC	Mg	1.2057	1.2057	279.0984	0.0279%
BC	Na	21.3964	21.3964	4952.8786	0.4953%
BC	S	0.7240	0.7240	167.5979	0.0168%
BC	Si	3.2645	3.2645	755.6802	0.0756%
BC	Ag	0.0027	0.0027	0.6231	0.0001%
BC	Al	0.9061	0.9061	209.7431	0.0210%
BC	As	0.0000	0.0000	0.0000	0.0000%
BC	Au	0.0000	0.0000	0.0000	0.0000%
BC	B	0.0000	0.0000	0.0000	0.0000%
BC	Ba	0.0070	0.0070	1.6198	0.0002%
BC	Be	0.0000	0.0000	0.0000	0.0000%
BC	Bi	0.0000	0.0000	0.0000	0.0000%
BC	Cd	0.0000	0.0000	0.0000	0.0000%
BC	Ce	0.0000	0.0000	0.0000	0.0000%
BC	Co	0.0000	0.0000	0.0000	0.0000%
BC	Cr	0.0227	0.0227	5.2583	0.0005%
BC	Cu	0.0000	0.0000	0.0000	0.0000%
BC	Dy	0.0000	0.0000	0.0000	0.0000%
BC	Er	0.0000	0.0000	0.0000	0.0000%
BC	Eu	0.0000	0.0000	0.0000	0.0000%
BC	Fe	0.7289	0.7289	168.7174	0.0169%
BC	Ga	0.0000	0.0000	0.0000	0.0000%
BC	Gd	0.1209	0.1209	27.9754	0.0028%
BC	Ge	0.0317	0.0317	7.3476	0.0007%
BC	Hf	0.0000	0.0000	0.0000	0.0000%
BC	Ho	0.0000	0.0000	0.0000	0.0000%
BC	In	0.0000	0.0000	0.0000	0.0000%
BC	Ir	0.0000	0.0000	0.0000	0.0000%
BC	La	0.0000	0.0000	0.0000	0.0000%
BC	Li	0.0000	0.0000	0.0000	0.0000%
BC	Lu	0.0000	0.0000	0.0000	0.0000%
BC	Mn	0.0267	0.0267	6.1820	0.0006%
BC	Mo	0.0046	0.0046	1.0593	0.0001%
BC	Nb	0.0030	0.0030	0.6995	0.0001%
BC	Nd	0.0000	0.0000	0.0000	0.0000%

BC	Ni	0.0031	0.0031	0.7151	0.0001%
BC	P	0.0213	0.0213	4.9231	0.0005%
BC	Pb	0.0000	0.0000	0.0000	0.0000%
BC	Pd	0.0000	0.0000	0.0000	0.0000%
BC	Pr	0.0000	0.0000	0.0000	0.0000%
BC	Pt	0.0000	0.0000	0.0000	0.0000%
BC	Re	0.0573	0.0573	13.2542	0.0013%
BC	Rh	0.0033	0.0033	0.7600	0.0001%
BC	Ru	0.0000	0.0000	0.0000	0.0000%
BC	Sb	0.0147	0.0147	3.3989	0.0003%
BC	Sc	0.0000	0.0000	0.0000	0.0000%
BC	Se	0.0000	0.0000	0.0000	0.0000%
BC	Sm	0.0101	0.0101	2.3336	0.0002%
BC	Sn	0.0000	0.0000	0.0000	0.0000%
BC	Sr	0.0058	0.0058	1.3325	0.0001%
BC	Ta	0.0096	0.0096	2.2120	0.0002%
BC	Tb	0.0000	0.0000	0.0000	0.0000%
BC	Te	0.0000	0.0000	0.0000	0.0000%
BC	Ti	0.0239	0.0239	5.5350	0.0006%
BC	Tl	0.0000	0.0000	0.0000	0.0000%
BC	Tm	0.0000	0.0000	0.0000	0.0000%
BC	V	0.0000	0.0000	0.0000	0.0000%
BC	W	0.0175	0.0175	4.0610	0.0004%
BC	Y	0.0410	0.0410	9.5009	0.0010%
BC	Yb	0.0000	0.0000	0.0000	0.0000%
BC	Zn	1.0299	1.0299	238.4022	0.0238%
BC	Zr	0.0380	0.0380	8.8026	0.0009%
BC	Hg	0.0025	0.0025	0.5737	0.0001%

Table S4. ICP-OES test results for the BC@UiO-66 separator.

Sample ID	Analyzed Element	Initial Solution Concentration C_0 (mg/L)	Digested Solution Concentration C_1 (mg/L)	Element Content C_x (mg/kg)	Element Content W (%)
BC@UiO-66	Ca	1.2845	1.2845	323.7078	0.0324%
BC@UiO-66	K	1.5558	1.5558	392.0938	0.0392%
BC@UiO-66	Mg	0.2884	0.2884	72.6709	0.0073%
BC@UiO-66	Na	1.3698	1.3698	345.2163	0.0345%
BC@UiO-66	S	0.2783	0.2783	70.1419	0.0070%
BC@UiO-66	Si	0.9532	0.9532	240.2250	0.0240%
BC@UiO-66	Ag	1.2697	1.2697	319.9943	0.0320%
BC@UiO-66	Al	3.9000	3.9000	982.8674	0.0983%
BC@UiO-66	As	0.0000	0.0000	0.0000	0.0000%
BC@UiO-66	Au	0.0000	0.0000	0.0000	0.0000%
BC@UiO-66	B	0.0103	0.0103	2.5951	0.0003%
BC@UiO-66	Ba	0.0023	0.0023	0.5880	0.0001%
BC@UiO-66	Be	0.0013	0.0013	0.3181	0.0000%
BC@UiO-66	Bi	0.0000	0.0000	0.0000	0.0000%
BC@UiO-66	Cd	0.0000	0.0000	0.0000	0.0000%
BC@UiO-66	Ce	0.2206	0.2206	55.5997	0.0056%
BC@UiO-66	Co	0.0000	0.0000	0.0000	0.0000%
BC@UiO-66	Cr	0.0377	0.0377	9.4936	0.0009%
BC@UiO-66	Cu	0.0000	0.0000	0.0000	0.0000%

BC@UiO-66	Dy	0.0000	0.0000	0.0000	0.0000%
BC@UiO-66	Er	0.0000	0.0000	0.0000	0.0000%
BC@UiO-66	Eu	0.0000	0.0000	0.0000	0.0000%
BC@UiO-66	Fe	0.4247	0.4247	107.0251	0.0107%
BC@UiO-66	Ga	0.0000	0.0000	0.0000	0.0000%
BC@UiO-66	Gd	0.0055	0.0055	1.3787	0.0001%
BC@UiO-66	Ge	0.0109	0.0109	2.7488	0.0003%
BC@UiO-66	Hf	4.9258	4.9258	1241.3858	0.1241%
BC@UiO-66	Ho	0.0313	0.0313	7.8947	0.0008%
BC@UiO-66	In	0.1172	0.1172	29.5367	0.0030%
BC@UiO-66	Ir	0.0000	0.0000	0.0000	0.0000%
BC@UiO-66	La	0.0000	0.0000	0.0000	0.0000%
BC@UiO-66	Li	0.0000	0.0000	0.0000	0.0000%
BC@UiO-66	Lu	0.0001	0.0001	0.0207	0.0000%
BC@UiO-66	Mn	0.0099	0.0099	2.4862	0.0002%
BC@UiO-66	Mo	0.0003	0.0003	0.0835	0.0000%
BC@UiO-66	Nb	0.0147	0.0147	3.7162	0.0004%
BC@UiO-66	Nd	0.7599	0.7599	191.5058	0.0192%
BC@UiO-66	Ni	0.0067	0.0067	1.6974	0.0002%
BC@UiO-66	P	0.0000	0.0000	0.0000	0.0000%
BC@UiO-66	Pb	0.0000	0.0000	0.0000	0.0000%
BC@UiO-66	Pd	0.3369	0.3369	84.9129	0.0085%

BC@UiO-66	Pr	0.0274	0.0274	6.9054	0.0007%
BC@UiO-66	Pt	0.0000	0.0000	0.0000	0.0000%
BC@UiO-66	Re	0.0598	0.0598	15.0643	0.0015%
BC@UiO-66	Rh	0.0000	0.0000	0.0000	0.0000%
BC@UiO-66	Ru	0.0000	0.0000	0.0000	0.0000%
BC@UiO-66	Sb	0.0000	0.0000	0.0000	0.0000%
BC@UiO-66	Sc	0.0000	0.0000	0.0060	0.0000%
BC@UiO-66	Se	0.0000	0.0000	0.0000	0.0000%
BC@UiO-66	Sm	0.0000	0.0000	0.0000	0.0000%
BC@UiO-66	Sn	0.1410	0.1410	35.5416	0.0036%
BC@UiO-66	Sr	0.0018	0.0018	0.4639	0.0000%
BC@UiO-66	Ta	0.0000	0.0000	0.0000	0.0000%
BC@UiO-66	Tb	0.0000	0.0000	0.0000	0.0000%
BC@UiO-66	Te	0.0000	0.0000	0.0000	0.0000%
BC@UiO-66	Ti	0.2051	0.2051	51.6957	0.0052%
BC@UiO-66	Tl	0.0000	0.0000	0.0000	0.0000%
BC@UiO-66	Tm	0.0000	0.0000	0.0000	0.0000%
BC@UiO-66	V	0.0107	0.0107	2.6928	0.0003%
BC@UiO-66	W	0.0058	0.0058	1.4710	0.0001%
BC@UiO-66	Y	0.0010	0.0010	0.2456	0.0000%
BC@UiO-66	Yb	0.0000	0.0000	0.0000	0.0000%
BC@UiO-66	Zn	0.2668	0.2668	67.2429	0.0067%

BC@UiO-66	Zr	4.4118	441.1781	111184.0005	11.1184%
BC@UiO-66	Hg	0.0068	0.0068	1.7018	0.0002%

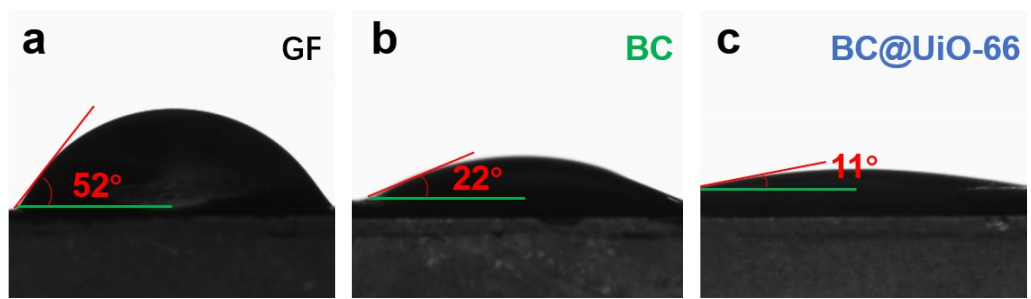


Figure S4. Contact angle test images of the separators: (a) GF separator, (b) BC separator, (c) BC@UiO-66 separator.

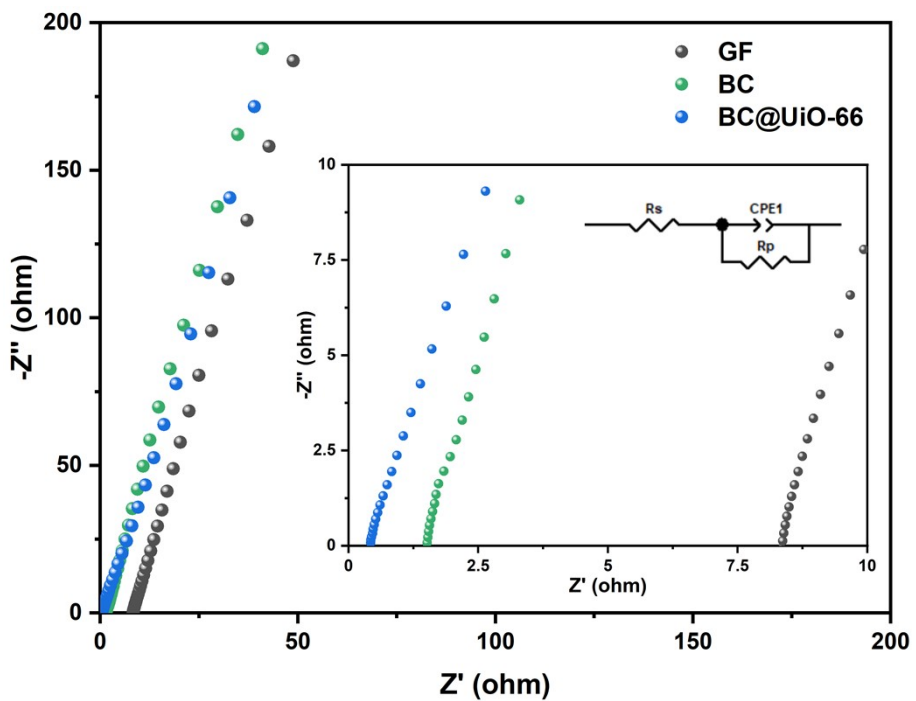


Figure S5. AC impedance of SS//SS battery test images of the separators: GF separator, BC separator, and BC@UiO-66 separator.

Table S5. The Rs and Rp impedance values of GF, BC, and BC@UiO-66 separators.

Sample	Rs	CPE-T	CPE-P	Rp
GF	8.331	0.000037917	0.89432	3105800
BC	1.506	0.000030804	0.87618	2966000
BC@UiO-66	0.42742	0.000039596	0.85555	1251600

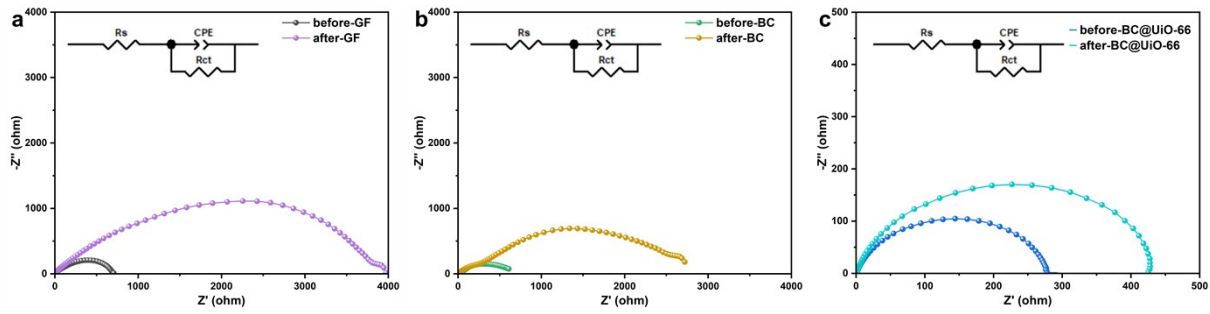


Figure S6. (a) AC impedance spectra of GF separator, (b) BC separator, and (c) BC@UiO-66 separator before and after polarization.

Table S6. The R_s and R_{ct} impedance values of GF, BC, and BC@UiO-66 separators.

Sample	R_s (before)	R_{ct} (before)	R_{ct} (after)
GF	7.45	701	3800
BC	3.07	610	2600
BC@UiO-66	0.7944	278.6	425.1

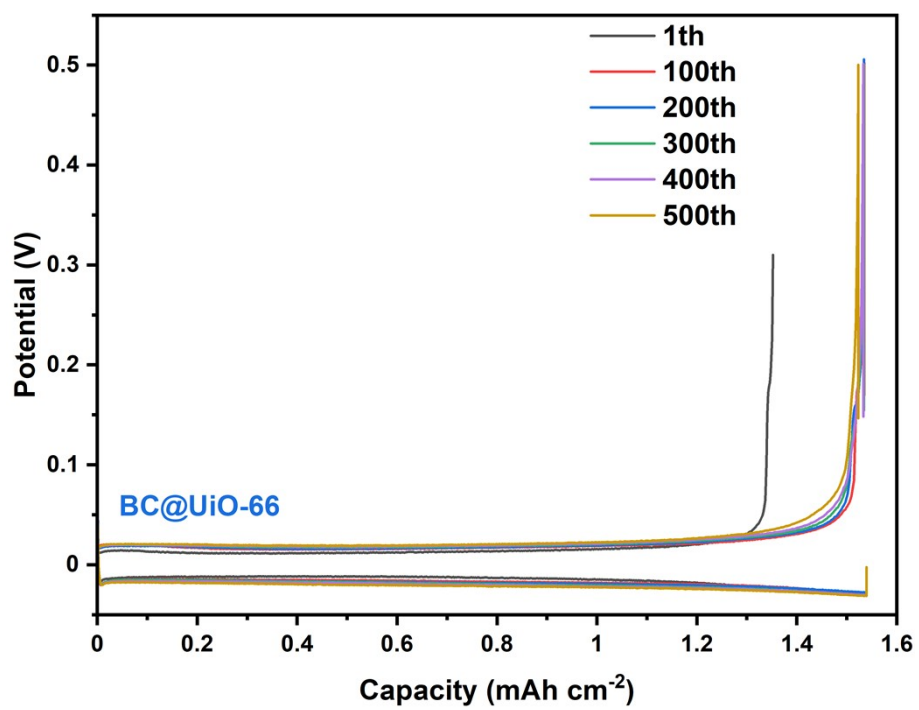


Figure S7. Capacity-voltage curves of the BC@UiO-66 separator after different numbers of cycles.

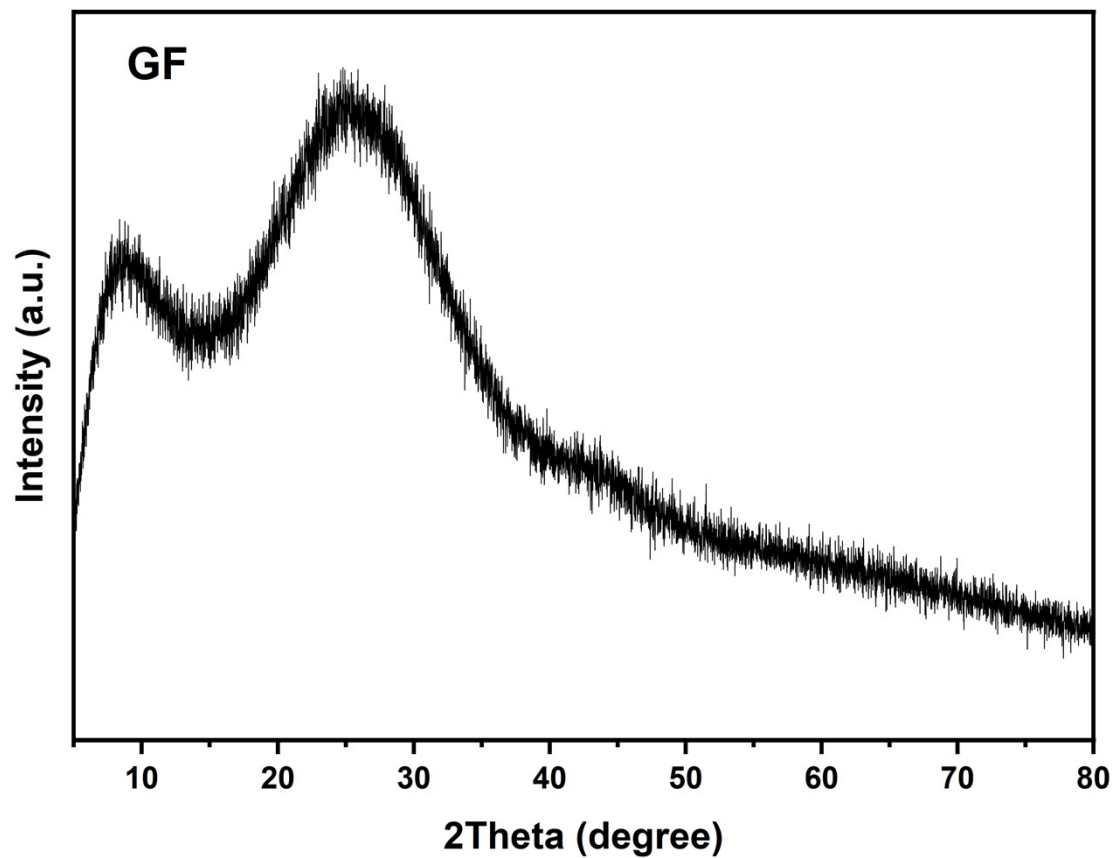


Figure S8. XRD pattern of GF.

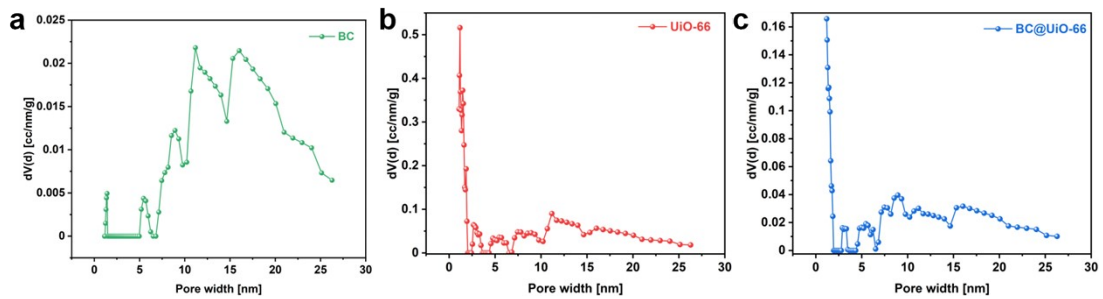


Figure S9. Pore size distribution diagrams of (a) BC separator, (b) UIO-66, and (c) BC@UIO-66 separator

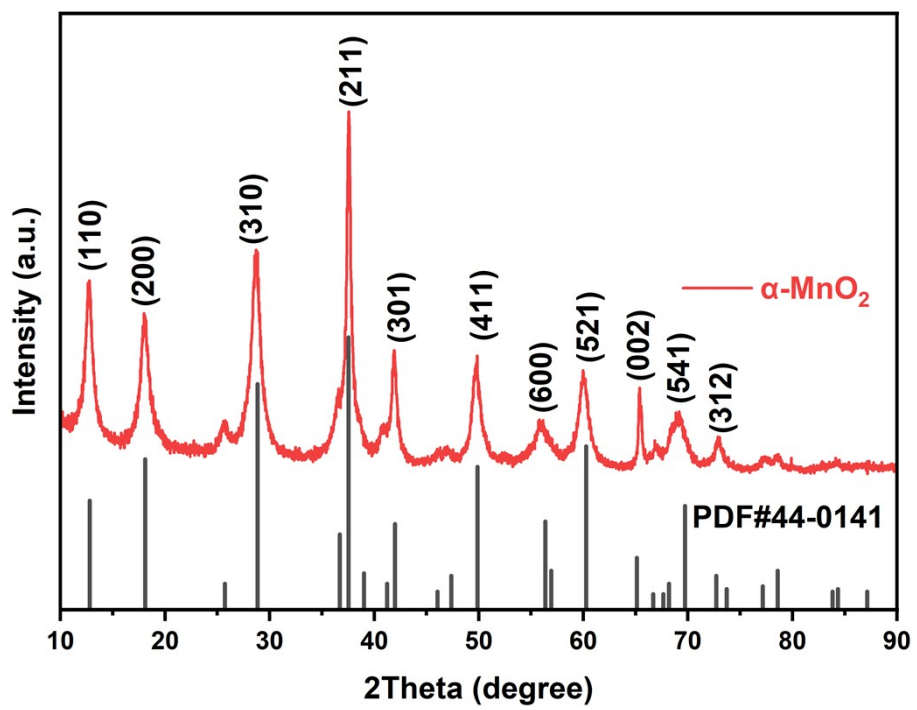


Figure S10. XRD pattern of α -MnO₂.

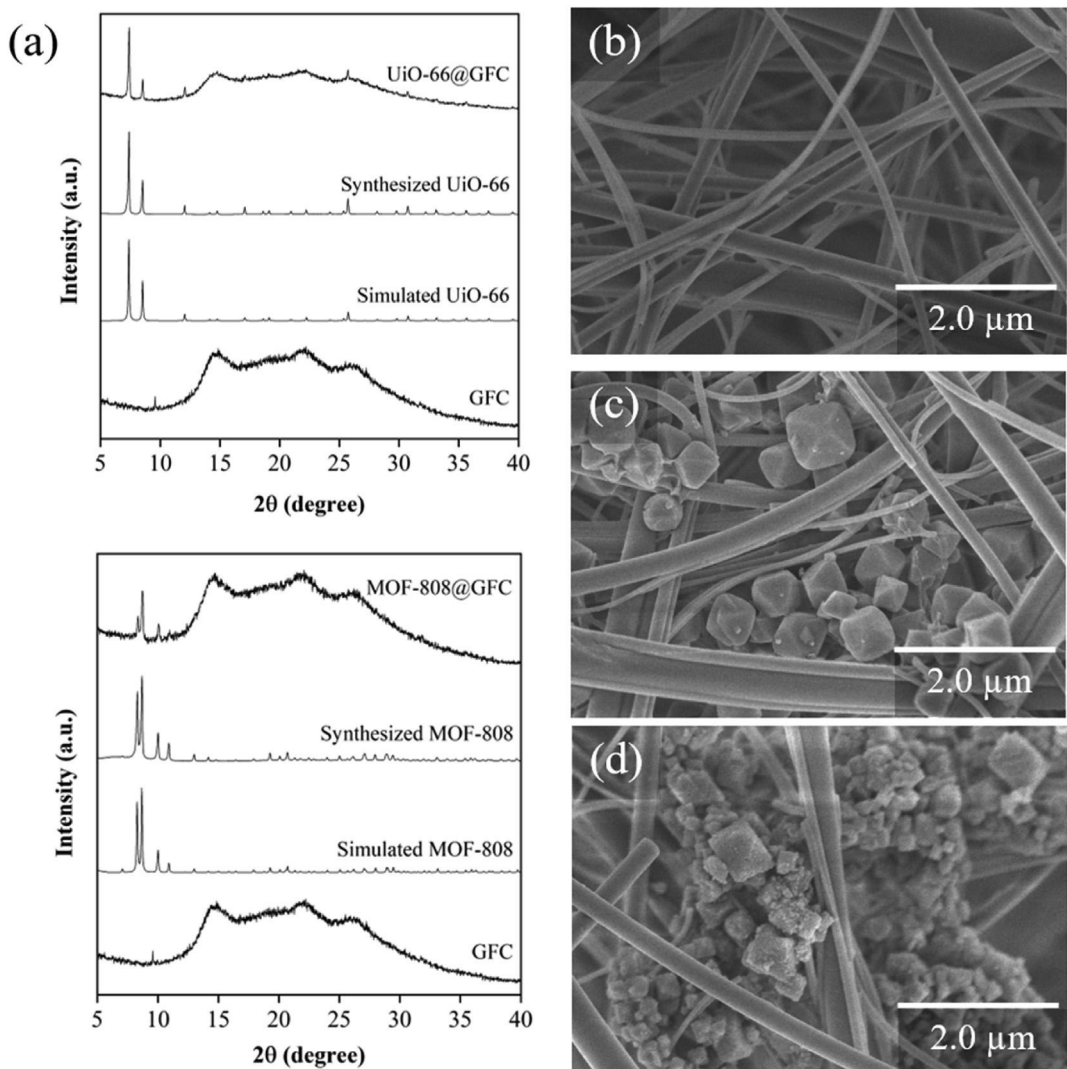


Figure S11. (a) XRD patterns of MOF-808@GFC and UiO-66@GFC, (b) SEM image of GF separator, (c) SEM image of UiO-66@GFC separator, (d) SEM image of MOF-808@GFC separator, Reprinted with permission from Ref.¹. Copyright 2022 Elsevier.

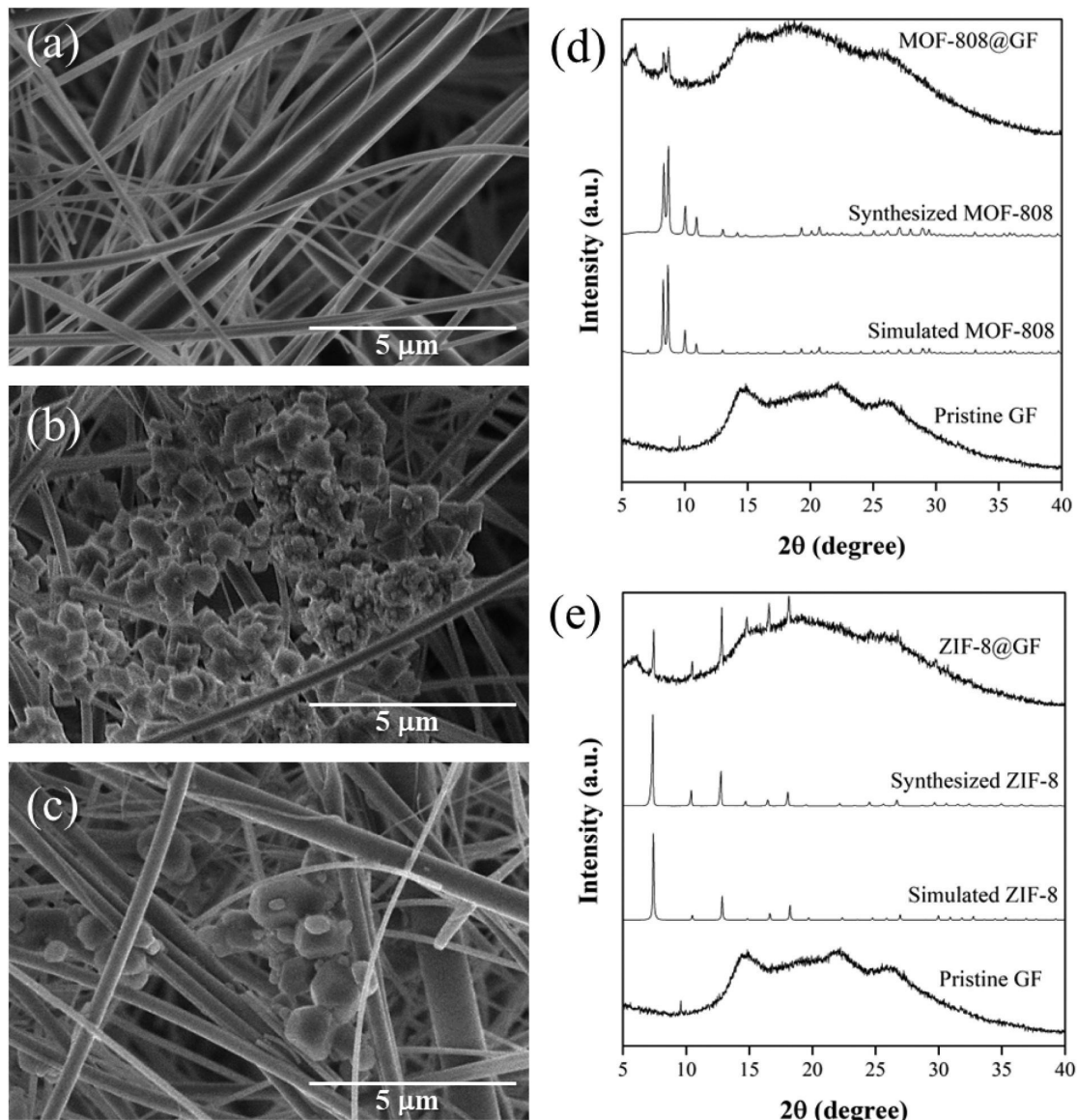


Figure S12. SEM images of (a) GF separator, (b) MOF-808@GF separator, (c) ZIF-8@GF separator, (d) XRD patterns of MOF-808@GF separator, (e) XRD patterns of ZIF-8@GF separator, Reprinted with permission from Ref.². Copyright 2024 Elsevier.

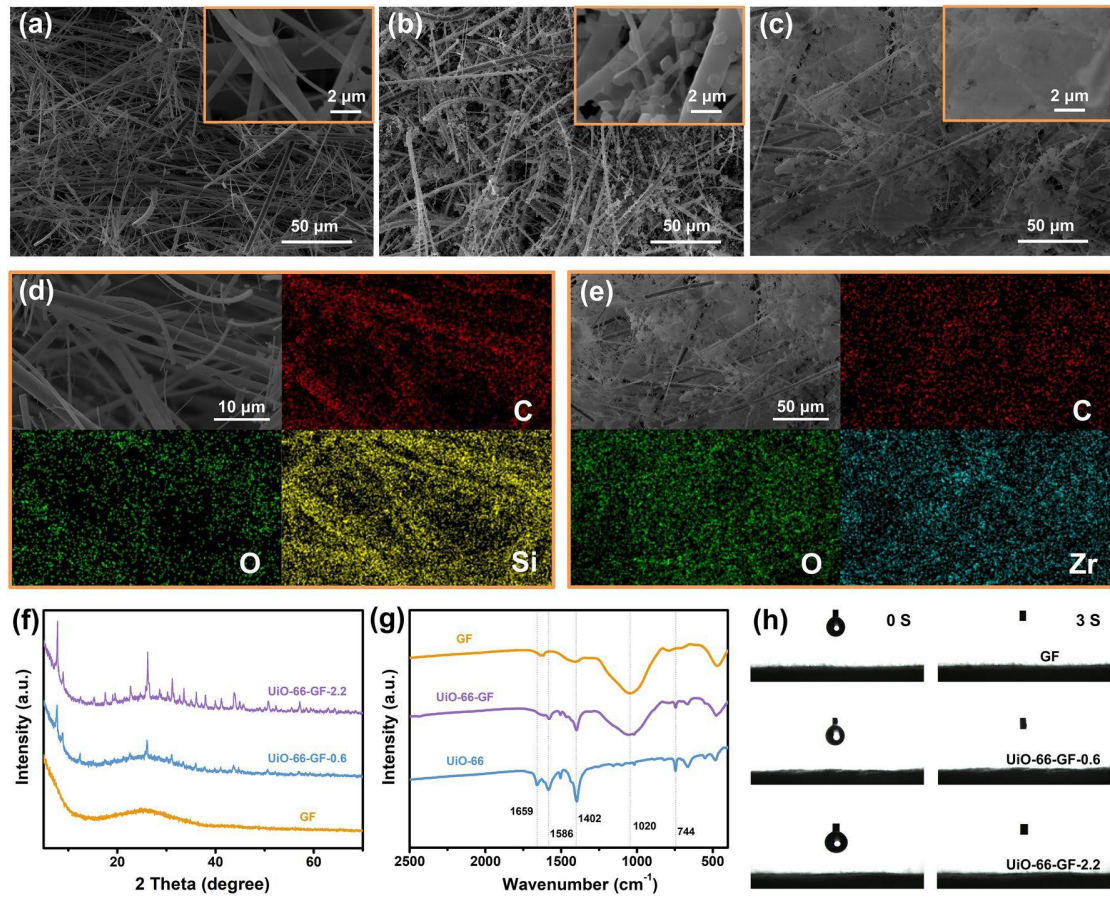


Figure S13. SEM images of (a) GF separator, (b) UiO-66-GF-0.6 separator, (c) UiO-66-GF-2.2 separator, (d) SEM image and element mapping of UiO-66-GF-0.6 separator, (e) SEM image and element mapping of UiO-66-GF-2.2 separator, (f) XRD patterns of GF, UiO-66-GF-0.6 and UiO-66-GF-2.2 separators, (g) FTIR spectra of GF, UiO-66-GF and UiO-66, (h) Contact angle tests for GF, UiO-66-GF-0.6 and UiO-66-GF-2.2 separators, Reprinted with permission from Ref. ³. Copyright 2022 Springer Nature.

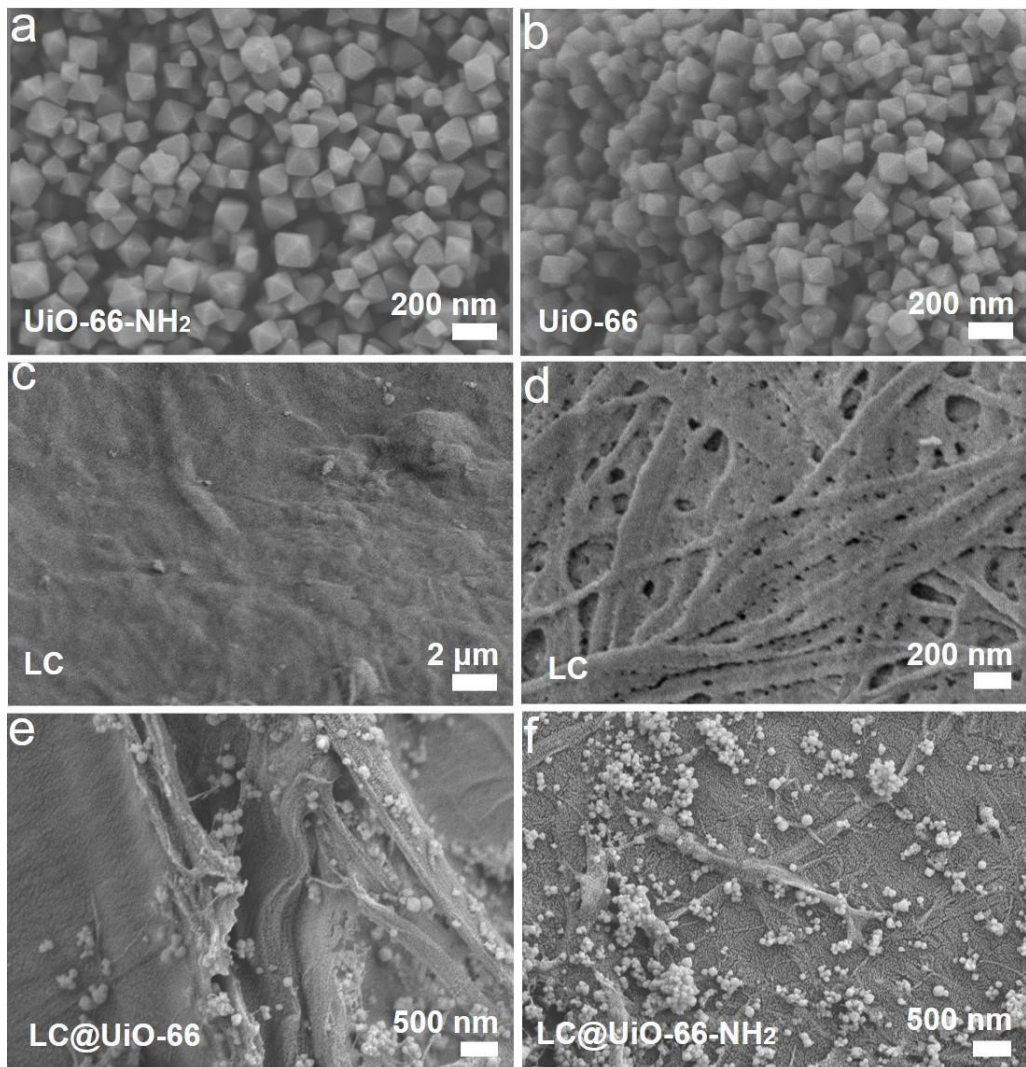


Figure S14. SEM images of (a) UiO-66-NH₂ particles, (b) UiO-66 particles, (c,d) LC separator, (e) LC@UiO-66 separator, (f) LC@UiO-66-NH₂ separator, Reprinted with permission from Ref. ⁴. Copyright 2023 Wiley.

Table S7. Comparison of BET surface areas of modified Separators.

Material	Synthesis Method	BET Surface Area (m ² /g)	Reference
UiO-66	Room Temperature Synthesis	1193.743	This work
BC@UiO-66	In Situ Growth	534.327	This work
UiO-66-NH ₂	Solvothermal Method	831	4
LC@UiO-66-NH ₂	Blending Method	132	4
UiO-66	Solvothermal Method	990.3	3
UiO-66	Solvothermal Method	1052.01	5
UiO-S1	Solvothermal Method	353.21	5
UiO-S2	Solvothermal Method	235.93	5
M-125	Solvothermal Method	221.5	6
NM-125	Solvothermal Method	925.2	6
CAU - 17	Solvothermal Method	634.28	7
ZIF-8	Hydrothermal method	938.2	8

Table S8. Comparison of Cycling Performance for Symmetric Batteries with Modified Separators.

Material	Current Density (mA/cm ²)	Capacity (mAh/cm ²)	Cycling Performance (h)	References
BC@UiO-66	1	1	2400	This work
BC@UiO-66	5	1	700	This work
GF-Ti ₃ C ₂ Tx	5	1	300	9
MOF-808@GFC	0.1		350	1
UiO-66	2	1	500	10
COOH/rGO interlayers				
CS@NGDY	5	1	500	11
PP/PE@MOF-rGO	2	1	500	10
PA-doped p-PBI	2	1	500	12
GF-PANI	2	1	250	13
Cellulose/g-C ₃ N ₄	3	1	600	14
MOF-NS/PAN	2		1400	15
ZnHAP/BC	1	1	1500	16
Zr-CNF	1	1	1600	17
UiO-66-GF	2	1	1650	3
Cellulose/GO	2	1	1750	18
LC@UiO-66-NH ₂	2	2	2000	4
CF	1	1	2000	19
ZrO ₂ /cellulose	0.5	0.25	2000	20
ZSM-5 molecular sieve	1	1	2000	21
BN@cellulose	0.3	0.3	1600	22
CT	1	0.5	1200	23
CRC	0.5	0.5	820	24

Reference:

1. N. Maeboonruan, J. Lohitkarn, C. Poochai, T. Lomas, A. Wisitsoraat, S. Kheawhom, S. Siwamogsatham, A. Tuantranont and C. Sriprachuabwong, *J. Sci.: Adv. Mater. Devices*, 2022, **7**, 100467.
2. N. Maeboonruan, J. Lohitkarn, C. Poochai, A. Tuantranont, P. Limthongkul and C. Sriprachuabwong, *J. Energy Storage*, 2024, **85**, 111063.
3. Y. Song, P. Ruan, C. Mao, Y. Chang, L. Wang, L. Dai, P. Zhou, B. Lu, J. Zhou and Z. He, *Nano-Micro Lett.*, 2022, **14**, 218.
4. H. Ma, J. Yu, M. Chen, X. Han, J. Chen, B. Liu and S. Shi, *Adv. Funct. Mater.*, 2023, **33**, 2307384.
5. R. Chen, G. Zhang, H. Zhou, J. Li, J. Li, L.-H. Chung, X. Hu and J. He, *Small*, 2024, **20**, 2305687.
6. Z. He, X. Zhu, Y. Song, B. Li, X. Xu, Z. Zhang, N. Zhao, Y. Liu, J. Zhu, L. Wang, L. Dai and H. Tian, *Energy Storage Mater.*, 2025, **74**, 103886.
7. Y. Shao, W. Lu, T. Zhang, B. Yin, B.-B. Xie, J. Ning and Y. Hu, *Carbon Energy*, 2023, **7**, e701.
8. W. Zhang, X. Zhu, L. Kang, Z. Peng, J. Zhu, L. Pan, L. Dai, S. Liu, L. Wang, Y. Liu and Z. He, *J. Energy Chem.*, 2024, **90**, 23-31.
9. J. Zhou, Z. Zhang, W. Jiang, S. Hou, K. Yang, Q. Li, L. Pan and J. Yang, *J. Alloys Compd.*, 2023, **950**, 169836.
10. Z. Wang, L. Dong, W. Huang, H. Jia, Q. Zhao, Y. Wang, B. Fei and F. Pan, *Nano-Micro Lett.*, 2021, **13**, 73.
11. Q. Yang, L. Li, T. Hussain, D. Wang, L. Hui, Y. Guo, G. Liang, X. Li, Z. Chen, Z. Huang, Y. Li, Y. Xue, Z. Zuo, J. Qiu, Y. Li and C. Zhi, *Angew. Chem. Int. Ed.*, 2022, **61**, e202112304.
12. Y. Lu, Y. Wen, F. Huang, T. Zhu, S. Sun, B. C. Benicewicz and K. Huang, *Energy Storage Mater.*, 2020, **27**, 418-425.
13. N. Zhao, Y. Zhang, Z. Zhang, C. Han, Y. Liang, J. Li, X. Wang, L. Dai, L. Wang and Z. He, *J. Colloid Interface Sci.*, 2023, **642**, 421-429.
14. Y. Yang, T. Chen, B. Yu, M. Zhu, F. Meng, W. Shi, M. Zhang, Z. Qi, K. Zeng and J. Xue, *Chem. Eng. J.*, 2022, **433**, 134077.
15. C.-Y. Liu, Y.-D. Wang, H. Liu, Q. Chen, X. Jiang, H. Jia and J.-P. Lang, *Composites, Part B*, 2024, **272**, 111227.
16. H. Qin, W. Chen, W. Kuang, N. Hu, X. Zhang, H. Weng, H. Tang, D. Huang, J. Xu and H. He, *Small*, 2023, **19**, 2300130.
17. S. Yang, Y. Zhang, Y. Zhang, J. Deng, N. Chen, S. Xie, Y. Ma and Z. Wang, *Adv. Funct. Mater.*, 2023, **33**, 2304280.
18. J. Cao, D. Zhang, C. Gu, X. Wang, S. Wang, X. Zhang, J. Qin and Z.-S. Wu, *Adv. Energy Mater.*, 2021, **11**, 2101299.
19. W. Zhou, M. Chen, Q. Tian, J. Chen, X. Xu and C.-P. Wong, *Energy Storage Mater.*, 2022, **44**, 57-65.
20. J. Cao, D. Zhang, C. Gu, X. Zhang, M. Okhawilai, S. Wang, J. Han, J. Qin and Y. Huang, *Nano Energy*, 2021, **89**, 106322.
21. J. Zhu, Z. Bie, X. Cai, Z. Jiao, Z. Wang, J. Tao, W. Song and H. J. Fan, *Adv. Mate*

- r.*, 2022, **34**, 2207209.
22. S.-J. Lee, J.-H. Choi, I. Hwang, M.-H. Ryu, K.-N. Jung, H.-g. Cho, J. In Lee and G. Park, *Electrochem. Commun.*, 2025, **172**, 107882.
23. P. Cao, H. Zhou, X. Zhou, Q. Du, J. Tang and J. Yang, *ACS Sustainable Chem. Eng.*, 2022, **10**, 8350-8359.
24. H. Zhang, J. Li, H. Ren, J. Wang, Y. Gong, B. Wang, D. Wang, H. Liu and S. Dou, *iScience*, 2024, **27**, 110237.